Multifold Bandwidth Improvement in Conformal Patch Antenna for Aircraft Application Using Corrugated Edge Coupling

Jeyakumar Monica* and Paramasivam Jothilakshmi

Department of Electronics and Communication Engineering
Sri Venkateshwara College of Engineering, Anna University, Pennalur, Sriperumbudur, Chennai, India
*jkumarmonica@gmail.com, jothi@svce.ac.in

Abstract ─ In the high-speed Internet of Things (IOT) era, the aircraft on-board is one of the few places that lacks high speed network access. The speed of this communication link between the ground station and the aircraft is limited by the transmitting antenna power, cost, latency and available infrastructure. The Direct Air to Ground (DATG) is a much-guaranteed technique which can provide a high-speed link between the ground station and aircraft. This paper describes a novel conformal microstrip patch antenna design which provides fourfold increase in bandwidth. As the bandwidth of an antenna mounted on the fuselage of aircraft is crucial to achieve higher data rate, this antenna performance is promising and suits better for DATG application. The proposed antenna with a size of (6.81 X 7.21cm) achieves a bandwidth of ~700MHz (5.032GHz to 5.73GHz) and max Gain of 9.53dB with max radiation efficiency of 93%. As this antenna is to be mounted on the aircraft fuselage, a substrate material, RT duroid 5880 with a thickness of 0.787mm is selected to have better conformability, low loss and high gain. This paper explains the different performance metrics involved in the DATG system and derives the specification for the proposed antenna structure. Also, the detailed structural analysis with the support of parametric and Characteristic Mode Analysis (CMA) is provided to get the physical insight of the designed antenna.

Index Terms ─ Characteristic mode analysis, direct air to ground, internet of things.

I. INTRODUCTION

The global liberalization of trade has increased the movement of people from one continent to another, one country to another and one city to another more frequently. The major medium of transport is through air, as it is more efficient in terms of travel time. The number of passengers as well as the number of carriers also growing year by year. The statistics [1] shows that more than 4.1 Billion passengers had been travelled in the commercial aircraft in 2017. Another statistic [2] shows that it may increase to 8.2 Billion in 2037. There are total of 1303 airlines all over the world which operates approximately 32000 fleets [3] per annum. As the business have spread throughout the world due to globalization, it has become necessary for the people to be connected in order to meet the deadlines, as the competition has grown exponentially. In this competitive world when someone does a business travel from one place to another, doesn't want to miss the business updates. Another aspect of internet availability inside the aircraft is streaming the videos, movies etc. to keep the kids engaged which helps in smooth travel experience with family.

The aircraft uses an on-board radio equipment with different types of antenna operating at different frequency bands. There are two broad classification of aircraft communication with respect to the distance of communication, Short range aircraft communication systems and Long-range communication systems [4]. The short-range communication uses Very High Frequency (VHF) band of 118 to 137MHz, to communicate with the air traffic control stations. The communication is limited to a line of sight (LOS) distance within the earth curvature change. The LOS distance for these short-range communications can be calculated as shown in [4]. Also, the antenna used for this communication is usually Omni-directional and vertically polarized with approximate power rating of 5 to 30W. The long-range communication is traditionally carried out through High Frequency (HF) band of 3 to 30MHz [4]. Since this communication channel supports the distance beyond the LOS distance, the transmitted waves undergo multiple reflections from the earth surface before reaching the destination, thus requires lot of power (300 – 1000W) in the transmitter.

Another method of long-range communication is adopted along with the development in satellite communication. In satellite communication method [5], the smaller aperture antenna arrays are mounted on top of the aircraft fuselage with the ability of rotating the main lobe direction in order to keep the connection intact while the carrier is moving. This method of satellite communication uses relatively lesser power. The major

Submitted On: January 13, 2021
Accepted On: May 17, 2021

https://doi.org/10.47037/2020.ACES.J.360512

drawbacks of the system are the limited data rates, latency and the cost. This communication system uses either Geostationary or Non-Geostationary orbital satellites. The communication link through satellite is inevitable for those aircrafts flying between continents which are separated by a large ocean surface. But, for those inter-continent aircraft there is another way to communicate with the ground station which is called Direct Air to Ground (DATG). In this method, the transmitter antenna is mounted in the bottom of aircraft fuselage through which it connects to a series of ground station antennas separated by a distance of ~10 to 200km. The antenna used for DATG should also have adaptive beam-forming feature to provide the continuous network connectivity.

The Electronic Communication Committee (ECC) has recommended few frequency bands to be used in DATG communication [6], [7]. These recommendations are the result of few case studies carried out by ECC. It is also mentioned that the frequencies below 6GHz is suitable for this communication. As this technology is not widely available around the world, there is no common frequency band available for this communication. In this design the frequency band of 5 to 5.8GHz is selected for designing the antenna. Every communication channel has three bands, up-link, down-link and guard band. Usually the up-link uses the higher frequency band as this require more power because of environmental loss. As of now the data rate of this DATG communication channel is limited to 3 to 4MHz [8]. In this design the targeted data rate is ~500Mbps in order to support the future need of live cock-pit video, remote control, flight data transmission, on-board internet access etc., This paper concentrates on a unit antenna design for DATG applications. As this antenna is intended to be mounted on the fuselage of aircraft, the conformability nature of the antenna is also important. So, the designed antenna in conformed to different radius of curvatures, 20 to 30cm, during the simulation and measurement. In order to achieve the conformability, the RT Duroid 5880 with a thickness of 0.787mm is used as a substrate material.

In this proposed work a novel structure of conformal micro-strip patch antenna is designed, fabricated and tested. It achieves better bandwidth to meet the DATG system requirement. Also, the maximum antenna gain of 10dB at 5.3GHz is achieved which helps in reducing number of elements in the final phased array. The design is carried out with RT Duroid 5880 as a substrate with a thickness of 0.787mm. The system requirements, antenna geometry, structural analysis of designed antenna with the help of parametric study and Characteristic mode analysis are presented in Section II. Experimental results are discussed in Section III and finally the conclusion and future work is discussed in Section IV.

II. DESCRIPTION OF THE ANTENNA STRUCTURE

A. System requirements

In DATG communication channel, both the Ground station (GS) and the aircraft are always in the LOS region. The important parameters of a communication system are path loss, required transmitter gain, modulation scheme, Bandwidth, coverage distance and transmitter gain. The path loss or fading is the time varying attenuation of the transmitted signal before reaching the receiver. This time varying attenuation is mainly because of the changing environment. It is important to know the path loss because the transmitting power has to be derived based on the path loss calculation. The path loss is dependent on the distance between the transmitter and the receiver. The mean path loss in free space is expressed below, [9,10]:

$$L(d) = 10 * \gamma * \log_{10}(d) + (20 - 10 * \gamma) * \log_{10}(d_0) + 20 * \log_{10}(f) + 32.5dB. \quad (1)$$

Where d is the distance between aircraft and GS (km), d_0 is the reference distance for which the path loss is known, 'f' is the transmitting signal frequency (GHz), 'γ' is the propagation constant (is 2 for free space). The above equation can be used to estimate the free space path loss at different frequencies and distance. For instance, with a separation of 80km and the signal frequency of 5.2GHz the path loss can be calculated as, ~145dB. The loss due to shadowing effect is not considered for this analysis.

The required bandwidth is dependent on the modulation scheme. For the required bit rate of 500Mbps, the needed bandwidth for different modulation scheme can be calculated using equation (2). The require bandwidths are, BPSK (M = 2) is 500MHz, QPSK (M=4) is 250MHz, QAM-16 (M=8) is 166MHz and QAM-64 (M=6) is 83MHz. Though the higher order modulation seems more efficient in terms of bandwidth, it has its own limitations such that the need of higher signal to noise ratio and bit more complicated receiver design. But the higher order modulation schemes help is accommodating large number of users within the available bandwidth. For instance, with QAM-64 and 700MHz transmitter bandwidth, approximately 8 users can access a speed of 500Mbps. As per the key performance indicators proposed for 5G DATG by NGMN Alliance [11] the required internet speed per user is estimated as ~15Mbps. If the fraction of achieved bandwidth 300MHz in combination with QAM-64 modulation scheme is assumed for the download link, then 120 on-board users can enjoy the internet speed of 15Mbps:

$$B = \left(\frac{R_b(1+a)}{\log_2 M}\right). \quad (2)$$

Where B is the transmitter bandwidth, R_b is the bit rate and M is the number of symbols used or constellation

points. The estimation of the signal to noise ratio is important because it helps in calculating the minimum signal power at the receiver and the required antenna gain to achieve it:

$$\mathrm{SNR} = \frac{E_b}{N_0} + 10\log_{10}\left(\frac{R_b}{B}\right) \text{ dB}. \quad (3)$$

Where E_b is the energy per Bit, N_o is the Noise power spectral density. The minimum signal power required at receiver end can be estimated using below equation, if the receiver system noise figure (NF) is known [12]. The noise figure parameter helps in identifying the amount of noise contributed by the components present in the receiver channel:

$$P_{RX} = \mathrm{SNR} * KT_0 * \mathrm{NF} * B. \quad (4)$$

Where P_{RX} is the Receiver power, SNR is the Signal to Noise ratio of the channel, K is the Boltzmann constant, T_o is the temperature (300K). The link budget equation for a LOS communication channel can be written as,

$$P_{RX} = P_{TX} - L_{TX} + G_{TX} - L(d) + G_{RX} - L_{RX}(\mathrm{dBm}). \quad (5)$$

Where P_{TX} represents the transmitted power, L_{TX} represents the transmitter system loss, G_{TX} represents the gain of the antenna mounted on aircraft fuselage, G_{RX} represents the Gain of the ground station antenna and L_{RX} represents the receiver system loss. This equation can be re-written to calculate the required gain of the antenna mounted on aircraft. By assuming typical values for the above-mentioned parameters, NF = 2dB, G_{RX} = 10dB, Bit error rate (BER) = 10^{-6}, L_{TX} = 10dB, L_{RX} = 5dB, the calculated values are SNR = 62dB, P_{RX} = -87dbm. From these values the required gain of the antenna is calculated as 36.28dB for a 1W of transmitted power. It falls down to 26.28dB if the transmitted power is 10W. These gain values are, to be achieved using the micro-strip phased array structure. The gain value of a unit element antenna in an array that determines the number of required elements and thus decides the antenna size [13]. So, achieving higher gain in a unit antenna helps in reducing the array size. Theoretically the gain increases by 3dB for every doubling of unit antenna element in the phased array. In order to achieve the required gain of 36.28dB the total number of unit antennas, with a gain of 10dB, needed are ~512. It is approximately a phased array structure of 24 X 24. The calculation in equation (6) shows the estimated transmitter antenna gain for the assumed conditions:

$$G_{TX} = -87\mathrm{dBm} - 30\mathrm{dBm} - 5.72 + 145 + 15 = 36.28\mathrm{dB}. \quad (6)$$

B. Antenna design

The geometry and CST design model of the proposed micro-strip patch antenna is shown in Figs. 1 and 2. Alike regular patch antenna, this proposed structure also has only three layers, ground plane, substrate and the top patch. It doesn't possess any defect in the ground plane as that technique is not suitable for the aircraft mounting. It uses RT Duroid 5880 as substrate with a thickness of 0.787mm in order to support the conformability. The top layer exhibits very distinct structural changes compare to its basic single patch antenna. The proposed antennas dimension is designed as per the design equations explained in [14]. The various dimensions of this proposed structure are explained below.

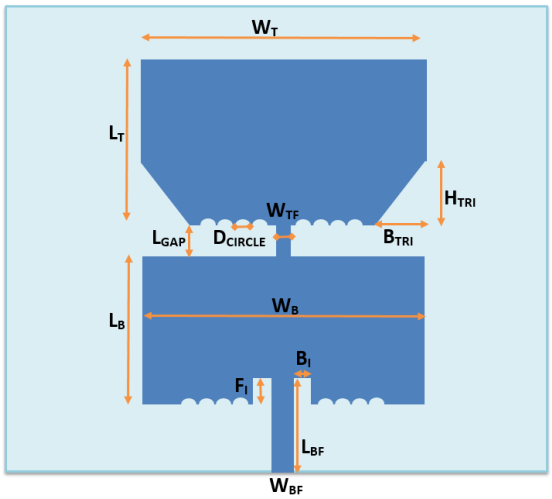

Fig. 1. Geometrical configuration of antenna structure.

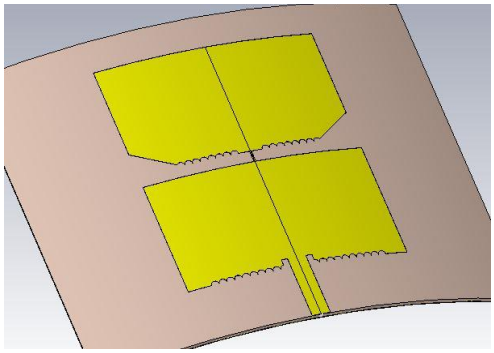

Fig. 2. CST simulation model of antenna structure.

Firstly, the bottom patch resembles the conventional single patch structure. L_B and W_B represents the length and width of the bottom patch. In this design inset feed is incorporated as it helps in easy integration with the other microwave circuitry. F_I and B_I illustrates the depth and the spacing of inset feed. W_{BF} and L_{BF} represents the width and length of the 50Ω micro-strip feed line. Secondly, there are two patches instead of one in the conventional single patch structure. The dimension of these two patches can be same or it differs slightly based on the final optimization. L_T and W_T illustrates the length and width of the top patch. The top patch is connected to the bottom patch through a small micro-strip

transmission line feed with a length L_{Gap} and width W_{TF}. Thirdly, the top patch has a triangular cut in the right and left bottom corners. The dimensions, height and breadth, of the right-angle triangular cuts are illustrated as H_{TRI} and B_{TRI}. The height and breadth of these cuts are not equal. Fourthly, the top and bottom patches exhibit multiple half circular cuts or wedges in its respective bottom edges. These circular cuts present in both the sides of the top and bottom feed line till the triangular edge. The number of cuts and its X-plane (Horizontal) location are same for both bottom and upper patches. The diameter of this circular cut is represented as D_{CIRCLE}. These circular wedges overlap with each other along its perimeter. The proposed structure is approximately double the size of single patch structure. But, this increase in size is outweighed by the benefit it provides, in terms of ~ 3dB increase in gain and approximately 4 times increase in bandwidth.

The Patch antenna is fed through a 50Ω microstrip feed to match the edge impedance. Then using the general patch antenna equations, the dimension of bottom and top patches are estimated. The feedline connecting both bottom and top patch is roughly sized as λ/20 and then optimized for better performance. The triangular cuts at the bottom has to be optimized to get dual resonance within the bandwidth. The spacing between the two patches has to be optimized for adding an additional resonance. The circular wedges are sized and spaced optimally to provide higher bandwidth.

The designed antenna measures 6.81cm (Length) * 7.21cm (Width) (inclusive of ground plane) is conformed to a curvature of 20-30cm to be placed in the aircraft fuselage.

C. Structural analysis

The bandwidth of the proposed structure is 700MHz that is approximately 13% of its center frequency, 5.4GHz. It is slightly more than four times the bandwidth of single patch antenna with same substrate thickness and material. This higher bandwidth is achieved through the structural changes mentioned above. In this section, the proposed antenna structure is disintegrated into multiple sub-structures and their return loss curve is observed for the resonance. Also, the parametric analysis is carried out for certain sub structures to get better understanding of the performance. It is also supported with the respective characteristic mode analysis results to get more physical insight of the behavior. For each sub structure the input is fed from the source with an impedance of 50Ω. These sub-structures are also conformed to a cylindrical fuselage made of Aluminum (Al) with a radius of curvature 25cm, in order to mimic the actual aircraft environment.

The first sub-structure to be analyzed is the standalone bottom patch without any circular cuts as shown in Fig. 3. This resembles the basic single patch antenna structure. The structure for analysis and its return loss curve is shown in Fig. 4. These simulation results clearly illustrate that this structure exhibits a single resonance at 5.16GHz. The return loss also has the second dip as the impedance is not properly matched with 50Ω feed. As it is a sub-structure, the impedance will change when it is integrated with other structural changes. Also, the CMA analysis is not critical for this single patch because it has a single feeding point through a micro-strip line which defines the current flow from the bottom edge to the top edge.

The second sub-structure is illustrated in Fig. 5. Structurally it exhibits a very minimal change of having small circular shape wedges at the bottom edge compared to a standalone single patch. As certain portion of copper is etched away in the bottom edge, it is expected to shift the resonant frequency upwards. Instead, it marginally reduces the resonant frequency to 5.12GHz as shown in Fig. 4.

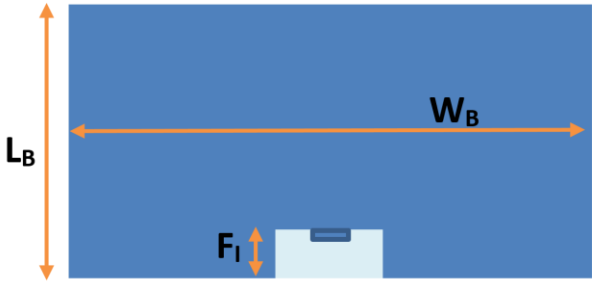

Fig. 3. Sub structure 1 - Bottom patch standalone.

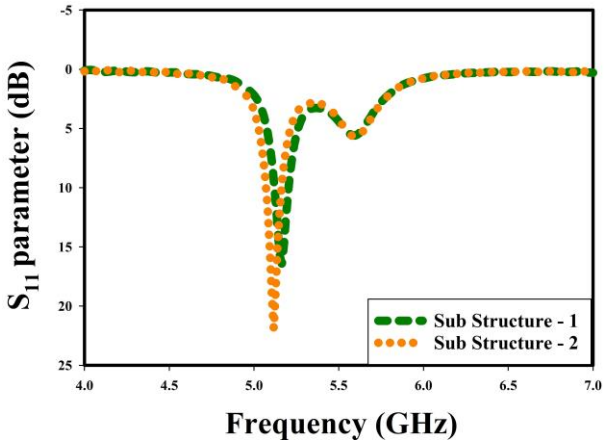

Fig. 4. Return loss curve - Structural changes in bottom patch.

The travel distance of the current in a patch decides the resonant frequency as the length of the patch is directly related to the wavelength. So, in order to reduce the resonant frequency, the current travel distance has to be longer than usual. Because of the presence of this circular wedges, certain portion of current components

travels around the perimeter of these circular wedges before resonating back. Therefore, the effective travel distance of the surface current is increased slightly. It can be clearly observed in the surface current plot shown in Fig. 6. The inclusion of this circular wedges helps in adjusting the resonant frequency slightly once this sub-structure is integrated into the proposed structure.

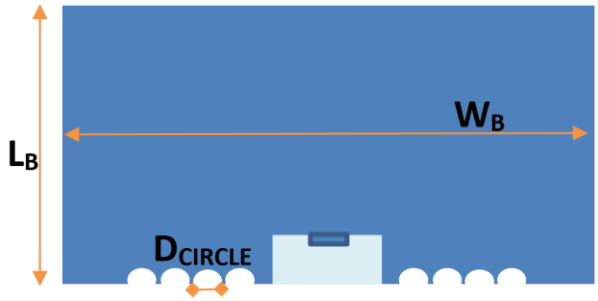

Fig. 5. Sub structure 2 - Bottom Patch with circular wedges.

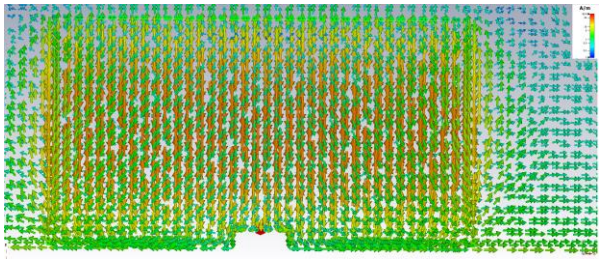

Fig. 6. Sub structure 2 - Surface current in the bottom patch with circular wedges.

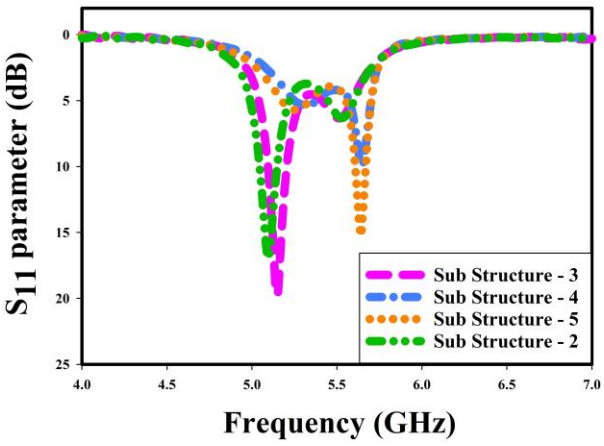

Fig. 7. Return loss curve - Structural changes in top patch.

The third sub-structure to be analyzed is the standalone top patch that has similar structure as standalone bottom patch shown in Fig. 3. The return loss curve corresponds to this structure is shown in Fig. 7. The length and width of this top patch structure matches with the standalone bottom patch dimensions. So, the resonant frequency of this structure, 5.15GHz is matching with the bottom patch. But this structure undergoes multiple structural changes unlike the bottom patch. The effect of these structural changes on top patch structure are discussed further in this section.

The fourth analysis is carried out on the sub-structure shown in Fig. 8. In this structure the rectangular patch is having a triangular cut in its bottom corners. The return loss curve corresponds to this structure is shown in Fig. 7. Though the return loss value is not higher than 10dB because of the standalone analysis, it provides information about the resonant points. The two resonant point are at 5.33GHz and 5.66GHz. The dimensions of this triangular cut also have significant impact on these resonant points. In order to understand the effect of H_{TRI} and B_{TRI}, parametric analysis is carried out and the results are shown in Fig. 9 and Fig. 10. Three major observations can be made from this parametric analysis. The first one is, the resonant point doesn't change much with both the parameters. The second observation is, as the B_{TRI} value comes closer or below the H_{TRI} value, the matching is good and the return loss curve goes above 10dB. It also indirectly means that the B_{TRI} modulates the edge impedance of the patch. The third observation is, as the H_{TRI} value moves closer or higher than B_{TRI} the resonance is lost. Based on these observations, it can be stated that the H_{TRI} has to be lesser than B_{TRI} to have a better matching with 50Ω source impedance.

So, these two parameters can be used as a trimming option in order to achieve optimized performance after the complete integration of structure. All the above observations are true only if the feed is provided at the bottom center edge and the current travels in the longitudinal direction. In the final integrated structure, this top patch is not fed directly by the source through micro-strip edge feeding instead it receives energy through the bottom patch. So, the direction of current entering into this top patch is not necessarily in longitudinal direction. So, carrying out an analysis using CMA will provide very useful insight on possible current flow directions on top patch and its corresponding resonant frequency. The details of CMA and its parameters can be found in literature [15-18]. The CMA is very useful in bringing up the hidden characteristics of patch antenna. The performance of any patch antenna has a direct relationship with the surface current flow. In CMA, different possible combinations of current flow are assumed and the corresponding parameters are estimated. These parameters are useful in fine tuning the antenna shape, size and feed location.

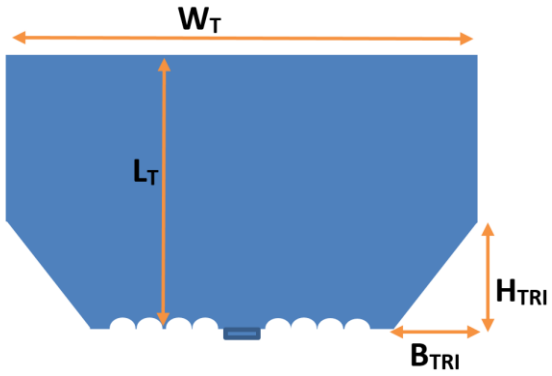

Fig. 8. Sub structure 4 - Top patch with triangular cuts.

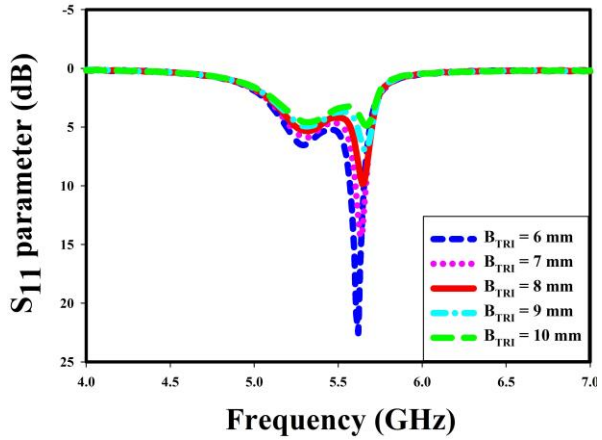

Fig. 9. Sub structure 4 - Return loss curve by sweeping B_{TRI} and H_{TRI} = 5.35 mm.

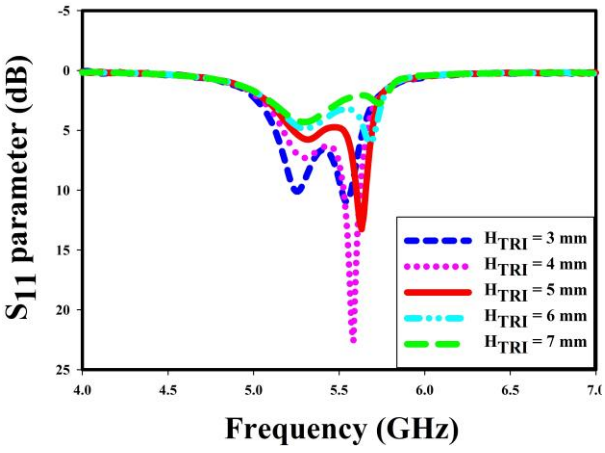

Fig. 10. Sub structure 4 - Return loss curve by sweeping H_{TRI} and B_{TRI} = 8 mm.

The vector form of characteristic mode is represented as follows,

$$X(\vec{J}_n) = \lambda_n R(\vec{J}_n). \quad (7)$$

Where $\vec{J}_n$ represents the Eigen characteristic current modes, λ_n is the eigen value, R and X are the resistive and reactive parts of impedance operator. Along with Eigen value (λ_n), the other two forms also used to estimate the characteristics of each current mode:

$$\text{Modal Significance (MS)} \; \alpha \; \frac{1}{1+j\lambda_n}, \quad (8)$$

$$\text{Characteristic Angle (CA)} = 180^{\circ} - \arctan(\lambda_n). \quad (9)$$

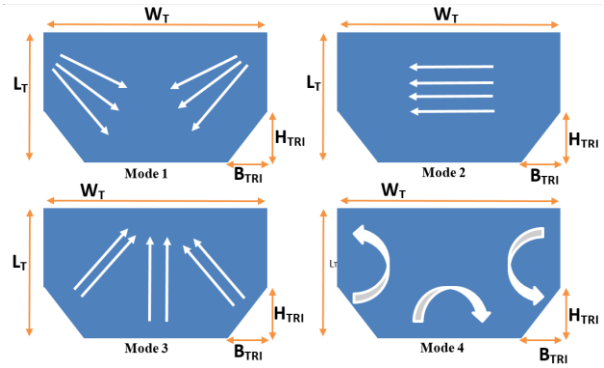

Fig. 11. Sub structure 4 - CMA current modes.

As this paper concentrates on bandwidth improvement, identifying the position of multiple resonant points are important. The resonant frequency of each current mode is represented differently by these three parameters.

1. Zero crossing frequency of Eigen value.
2. Peak frequency of Modal Significance.
3. 180˚ crossing frequency of CA.

In this paper only Modal Significance (MS) parameter and the respective surface current plots are used for analysis. Figure 11 and Fig. 12 show the different current modes and its corresponding MS curve across frequency. The frequency at which the MS curve reaches its peak value of unity depicts the resonant point of that particular current mode. The different current modes show the assumed direction of the surface current components.

This analysis clearly explains that the top patch structure can exhibit multiple resonant points depends on the direction and length of the current flow. The resonant point corresponds to mode 1 matches closely with the sub-structure of standalone edge fed top patch without any structural changes. The mode 3 exhibits matched resonant frequency with the sub-structure of standalone top patch with triangular cuts. The mode 4 resonates at much higher frequency as the current path is very short. So, it is very much clear that the top patch can have multiple resonant points depending on the direction of current injection.

The fifth sub-structure to be analyzed is the standalone top patch with both triangular cut and the circular wedges is shown in Fig. 13. The presence of

circular wedges slightly reduces the resonant frequency as shown in Fig. 7. The impact of the radius of these circular wedges are analyzed as a part of next sub structure.

The sixth structure to be analyzed is the integrated top and bottom patch without any structural modifications is shown in Fig. 14. The corresponding return loss curve is shown in Fig. 15. In this structure, the two patches with same dimensions are stitched together vertically through a narrow micro-strip line. The energy from the source has to travel through the bottom patch before exciting the top patch. So, there is a higher possibility that the top patch can receive the energy in different path and direction. One of such known paths is through the feed line connecting the two patches and another is through the overlapping edges. So, the important parameter to be analyzed in this structure is the gap between top and bottom patch and the width of the narrow feed line. The return loss graph is obtained for different gap values through simulation as shown in Fig. 16. Lowering the gap separates two resonant points and increasing the gap brings the two resonant points closer. This observation is very straightforward as the gap increases the magnitude of parasitic capacitance between the bottom and top patch reduces and thus turning this structure into a single patch. Therefore, further increase in gap merges the two resonant points into one. Another important parameter is the width of the feed line connecting two patches. The return loss curve is observed for different values of this feed line width. The parametric result is shown in Fig. 17. It can be observed that the change in width alters only the matching, i.e., the edge impedance at the input port.

The analysis of sixth sub-structure is further extended with CMA. Figure 18 shows 4 different current modes having a resonant frequency in the vicinity of expected bandwidth range. In the first current mode the current travels mostly in the lower patch and the amount of energy transferred to the upper patch is less. In the second current mode the current distribution is approximately equal in both the patches which means that there is a coupling between lower patch and the upper patch. This is directly visible from the resonant points of respective modes shown in Table 1, where the first mode possesses higher resonant frequency compare to the second mode. In third mode the current travels diagonally towards the horizontal edges, in both top and bottom patches, and thus the travel distance is less that results in little higher resonant frequency. In fourth current mode the current travels from one corner of the patch to another which results in shorter distance and thus results in higher resonant frequency. Also, the current distribution in both lower and upper patch is same in the fourth current mode. The separation between the mode 3 and mode 4 resonant point is ~280MHz in this structure. Similarly, the separation between mode 1 and mode 3 resonant point is ~290MHz. In order to keep the return loss higher than 10dB the resonant points have to be placed within a certain optimum distance. This structure tends to keep more distance between the resonant points and thus resulting in return loss below 10dB within the bandwidth. In order to improve the bandwidth, the placement of multiple resonant points has to be closer.

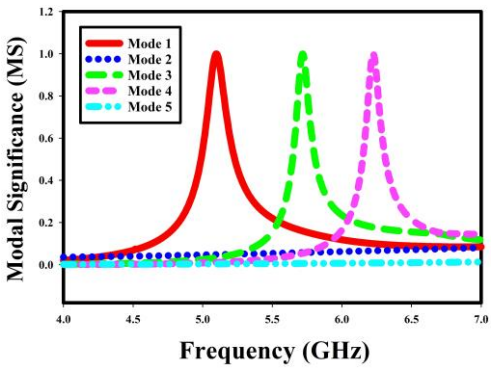

Fig. 12. Sub structure 4 - Modal significance curve.

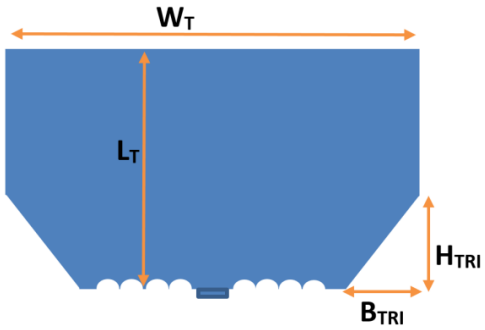

Fig. 13. Sub structure 5 - Top patch with triangular cuts and circular wedges.

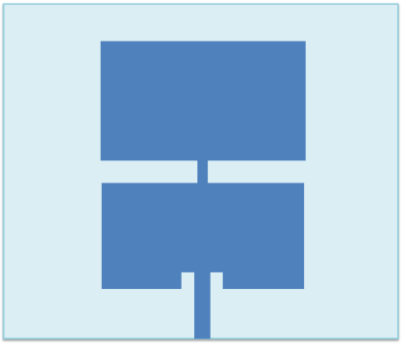

Fig. 14. Sub structure 6 - Integrated patch without any structural changes.

The seventh structure is the integrated top and bottom patch with triangular cuts on the bottom corner of top patch as shown in Fig. 19. The return loss curve

for this structure is shown in Fig. 15. This structure has slightly lesser bandwidth compare to the final structure. The respective current modes and its modal significant curves are shown in Fig. 20 and Fig. 21. The resonant points for each sub structure is listed in Table 1 and Table 2. This structure moves the mode 1 resonant point towards the mode 3 resonant point whereas the mode 3 resonant point is moved towards the mode 4 resonant point. Thus, the distance between mode 3 and mode 1 resonant point is further increased to ~330MHz. So, this structure tends to exhibit better performance but the middle portion of return loss curve bump towards 10dB point. The distance between each resonant point for all these sub-structures can be obtained from summary Table 2. Another important observation is that this structure lacks a resonant point in between and thus providing lesser bandwidth. Also, the return loss curve is hovering around the threshold point of 10dB. This is a result of widely separated resonant points. Therefore, an optimized structure should possess more resonant points spaced efficiently in order to get better bandwidth.

The next sub structure shown in Fig. 22, is the full integrated structure with only circular wedges at the bottom edge of top and bottom patch. This eighth structure exhibits similar behavior as the sixth structure except there is a little shift in the lower resonant points as shown in Table 2. The important parameter of this sub-structure is the diameter of the circular wedges. The parametric study is carried out by varying the diameter of circular wedges in this sub-structure and the corresponding return loss curve is shown in Fig. 23. The parametric study shows that the diameter of these circular wedges affects the lower resonant points and thus moves the lower resonant points towards lower frequency as the diameter increases.

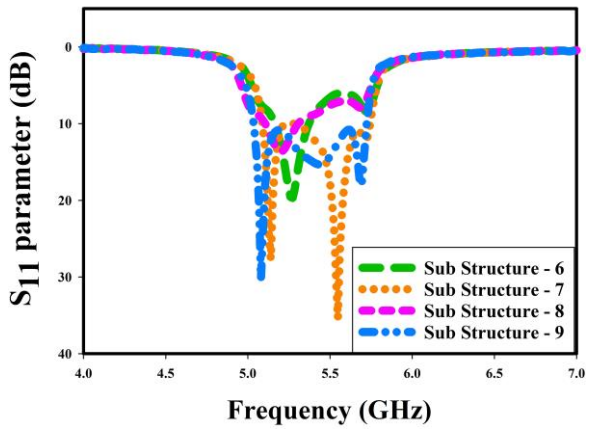

Fig. 15. Return loss curve - Integrated structure with different structural changes.

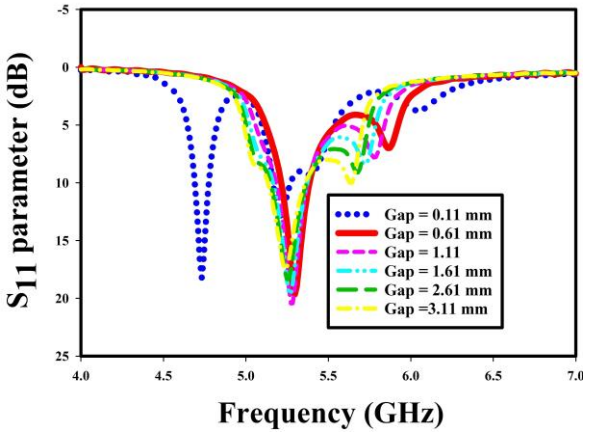

Fig. 16. Sub structure 6 - Return loss of parametric analysis L_{GAP}.

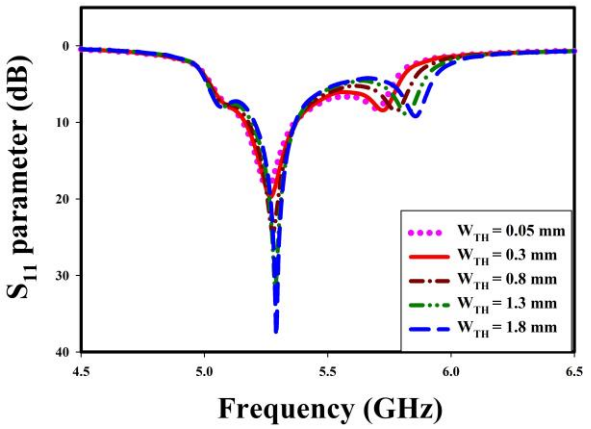

Fig. 17. Sub structure 6 - Return loss of parametric analysis W_{TF}.

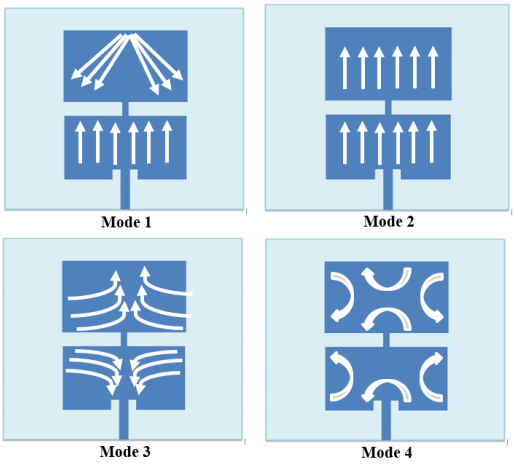

Fig. 18. Sub structure 6 - CMA current modes.

The ninth and final structure is the complete integrated structure with all the modifications as shown in Fig. 1. The return loss curve in Fig. 15, shows that this integrated structure possesses better bandwidth compare to all other sub structures. Also, the MS curve from the CMA analysis shows that the resonant points of four different current modes in Table 2 are spaced approximately at an equal distance. The distance between mode 1 and mode 2 resonant point is ~210MHz. The distance between mode 1 and mode 3 resonant point is ~270MHz. The distance between mode 3 and mode 4 resonant point is ~170MHz. This clearly explains the reason for exhibiting better performance compare to other sub structures.

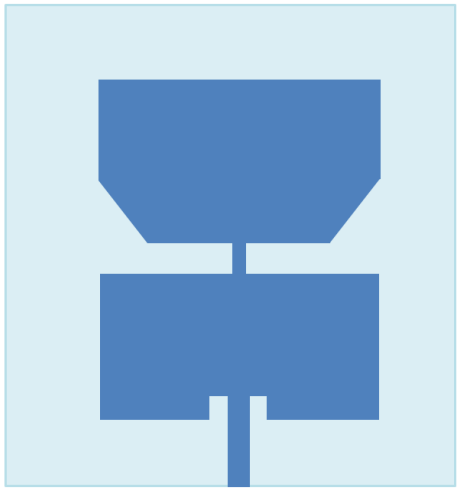

Fig. 19. Sub structure 7 - Integrated patch with only triangular cuts.

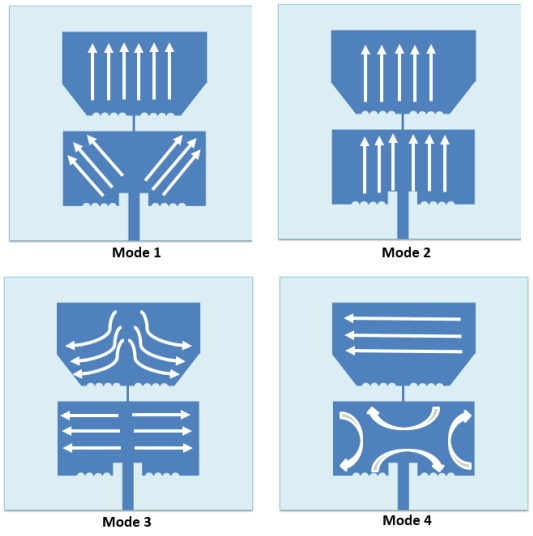

Fig. 20. CMA current modes for sub-structures 7, 8 and 9.

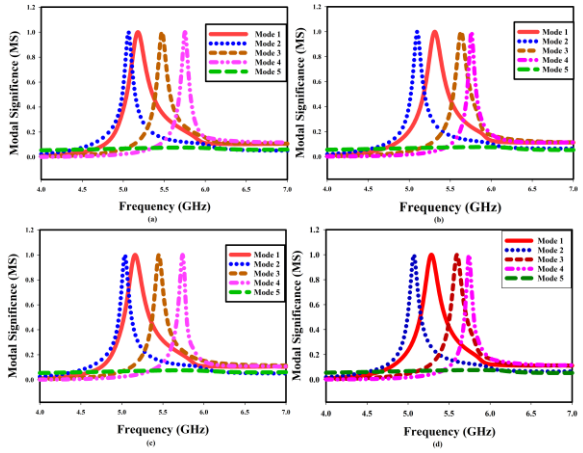

Fig. 21. CMA modal significance curve for sub-structures: (a) 6, (b) 7, (c) 8, and (d) 9.

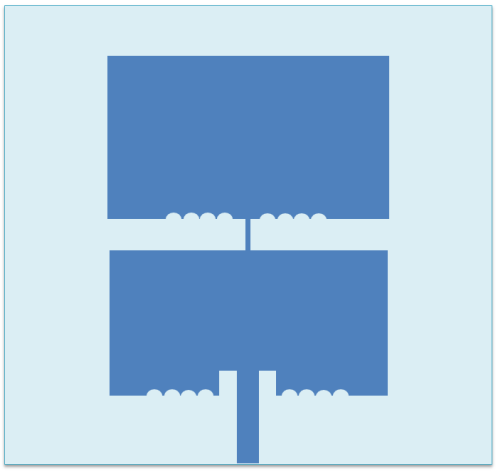

Fig. 22. Sub structure 8 - Integrated patch with only circular wedges.

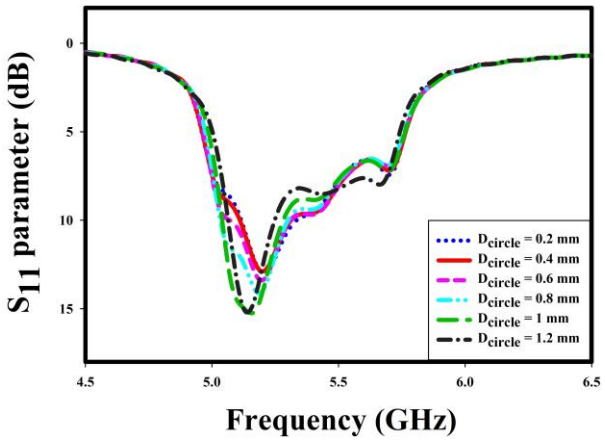

Fig. 23. Sub structure 8 - Return loss curve by sweeping D_{circle}.

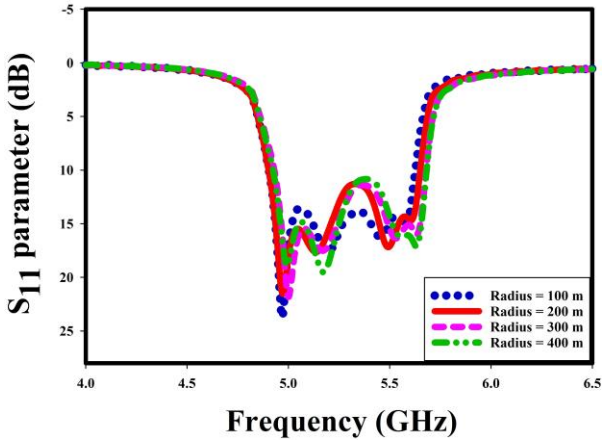

Fig. 24. Sub structure 9 - Return loss curve by sweeping the radius of curvature of fuselage.

Table 1: Resonant points of sub-structures 1 to 5

Sub Structure	1	2	3	4	5
Frequency (GHz)	5.16	5.12	5.16	5.33 & 5.66	5.08

Table 2: Resonant points of sub-structures 6 to 9 obtained through CMA

Sub Structure	6	7	8	9
Mode1 (GHz)	5.18	5.21	5.16	5.3
Mode2 (GHz)	5.063	5.1	5.035	5.074
Mode3 (GHz)	5.47	5.64	5.45	5.57
Mode4 (GHz)	5.756	5.76	5.74	5.74
Mode5 (GHz)	x	x	x	x

As this antenna is meant for aircraft application and will be mounted on the aircraft fuselage in the end application, it is important to analyze the return loss curve for different radius of curvature. The return loss curve for different radius of curvature is shown in Fig. 24. At different radius of curvature, the separation between the intermediate resonant points tend to move and bumps the return loss curve towards 10dB point. Still the return loss magnitude is kept higher than 10dB within the bandwidth. To improve the performance further across different radius of curvature, the parameters has to optimized independently for each radius of curvature.

III. RESULTS AND DISCUSSIONS

The proposed design is manufactured and tested for its performance. The manufactured antenna is conformed on top of two different cylindrical structures made of Aluminum (Al) and Carbon Fiber Composites (CFC) before taking the measurement as shown in Fig. 25. Mounting on these materials is very important because in the actual application this antenna is intended to be mounted on the aircraft fuselage. The aircraft fuselage is made of these composite materials in order to reduce the weight and thus to improve the payload [19]. The conventional techniques (e.g., increasing the thickness of substrate and Defected ground structure) used for improving micro-strip antenna bandwidth is not suitable for aircraft applications as the structure needs to support the conformability and also the fuselage is made of electrically conducting material (Al & CFC).

The return loss performance is measured with the help of network analyzer and the result is shown in Fig. 26. The measured return loss curves with both Al and CFC as fuselage, show good agreement with simulation results. This specific design achieves approximately 400% more bandwidths compare to a single patch antenna with a same substrate material and thickness. The maximum measured gain of 9.53dB is 76% more than a single patch gain of 7.1dB. It helps in reducing the transmitter power. The gain characteristics of the proposed antenna with different fuselage material mount is included in the Table 3. The measured antenna gain and the radiation efficiency at different frequency points inside the bandwidth is shown in Fig. 27. The reason for the difference in gain across frequency is the variation in current flow. The gain is more at frequencies where the current flows in both the patches and the gain is less where the current flows in only one patch. The radiation pattern of the antenna is depicted in Fig. 28 and Fig. 29.

The power requirement of the system is estimated again using the equations 1 to 6. With the proposed antenna having a gain of 9.53dB, the required transmitter power is calculated to be ~600W. Assuming a formation of 23X23 phased array structure with the proposed antenna, the estimated gain would be ~36.53dB. Therefore, it would require approximately 1W of transmitting power for this phased array structure.

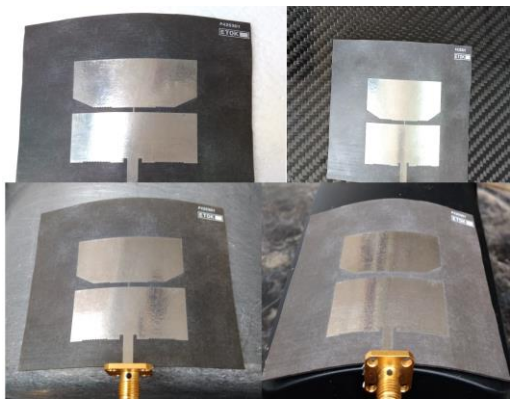

Fig. 25. Fabricated antenna conformed to aluminum and CFC cylindrical structure.

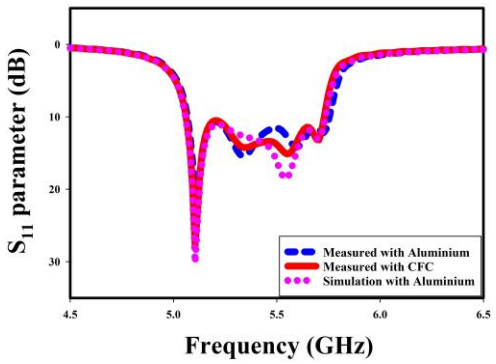

Fig. 26. The measured and simulated return loss plot of the antenna.

Table 3: Gain characteristics of proposed antenna at 5.3GHz with different substrate materials

Simulation/ Measured	Fuselage Material	Gain (dB)	Efficiency (%)
Simulation	Aluminum	9.3	92.7
Measured	Aluminum	9.15	92.5
Measured	CFC	9.53	93

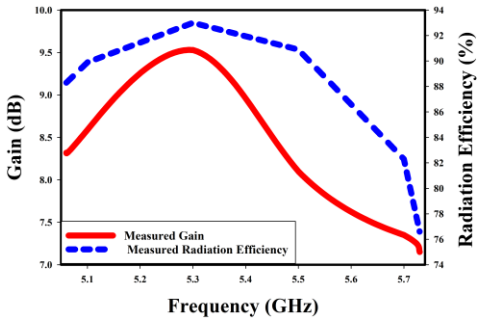

Fig. 27. Gain and efficiency curve across bandwidth.

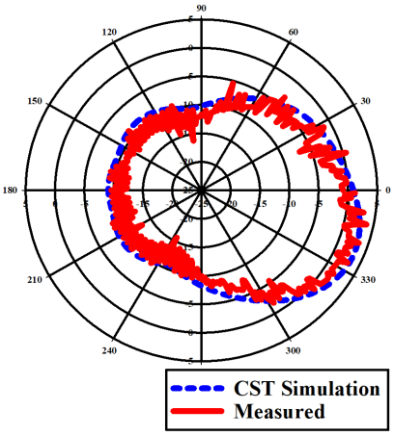

Fig. 28. Radiation pattern E-co.

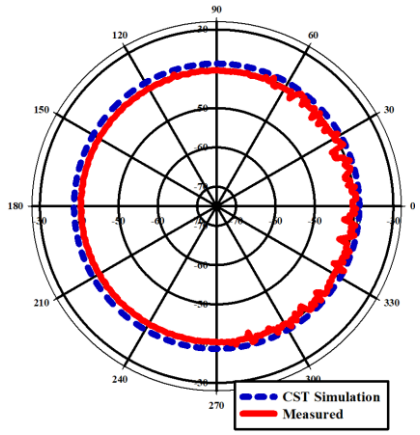

Fig. 29. Radiation pattern H-cross.

IV. CONCLUSION

A unit conformal micro-strip patch antenna is designed to provide a bandwidth of 700MHz and a gain of 9.53dB. With the increased bandwidth and conformal nature this design perfectly suits for DATG application. The achieved bandwidth helps in improving the data rate of internet connectivity inside the aircraft. The simulation results and measurement data are closely matching. In future, this work can be extended to phased array with beam steering capability. This phased array can be integrated into a DATG system to provide high speed internet or a communication link between the ground station and the aircraft. Also, this proposed structure can be analyzed further by changing the circular wedges and triangular cuts into different shapes to improve the performance.

REFERENCES

[1] D. Martinez, B. Ebenhack, and T. Wagner, *Energy Efficiency - Concepts and Calculations*, Elsevier Science Inc., May 10, 2019.

[2] S. K. Kearns, T. J. Mavin, and S. Hodge, *Engaging the Next Generation of Aviation Professionals*, Taylor and Francis Group, London, Nov. 8, 2019.

[3] T. Cooper, I. Reagan, C. Porter, and C. Precourt, *Global Fleet & MRO Market Forecast Commentary 2019–2029*, Oliver Wyman, Jan. 14, 2019.

[4] C. Binns, *Aircraft Systems: Instruments, Communications, Navigation, and Control*, John Wiley & Sons, Inc., New Jersey, Oct. 12, 2018.

[5] D. Stacey, *Aeronautical Radio Communication Systems and Networks*, John Wiley & Sons, Inc., New Jersey, Feb. 22, 2008.

[6] "Harmonised Standard for access to radio spectrum, Broadband Direct Air-to-Ground Communications; Equipment operating in the 1900 MHz to 1920 MHz and 5 855 MHz to 5 875 MHz frequency

bands; Beam-forming antennas," *Harmonised European Standard*, ETSI EN 303 316 V1.2.0 (2017-11).

[7] "Compatibility/sharing studies related to PMSE, DECT and SRD with DA2GC in the 2 GHz unpaired bands and MFCN in the adjacent 2 GHz paired band," *Electronic Communication Committee*, Approved Sep. 2014.

[8] "Systems for public mobile communications with aircraft-M Series Mobile, radio determination, amateur and related satellite service," *ITU-R M.2282-0 Electronic Publication*, Geneva, 2014.

[9] L. Ahlin and J. Zander, "Principles of Wireless Communications," *Student Litterateur*, Sweden, 1998.

[10] A. W. Graham, N. C. Kirkman, and P. M. Paul, *Mobile Radio Network Design in the VHF and UHF Bands: A Practical Approach*, John Wiley & Sons Ltd., Nov. 17, 2006.

[11] R. El Hattachi and J. Erfanian, "5G white paper," *NGMN Alliance*, ver. 1.0, Feb. 17, 2015.

[12] Avionics Department of Naval Air Warfare Center Weapons Division (NAWCWD TP 8347), *Electronic Warfare and Radar Systems Engineering Handbook*, Fourth Edition, Point Mugu, CA 93042, Oct. 2013.

[13] S. Alam, E. Wijanto, B. Harsono, F. Samandatu, M. Upa, and I. Surjati, "Design of array and circular polarization microstrip antenna for LTE communication," *MATEC Web of Conferences (ICIEE-2018)*, vol. 218, 2018.

[14] J. Monica and P. Jothilakshmi, "Gain enhanced conformal patch antenna with defected ground for aircraft applications," *IET Communications*, vol. 14, no. 2, pp. 290-299, Jan. 2020.

[15] M. Cabedo-Fabres, E. Antonino-Daviu, A. Valero-Nogueira, and M. Ferrando Bataller, "The theory of characteristic modes revisited: A contribution to the design of antennas for modern applications," *IEEE Antennas and Propagation Magazine*, vol. 49, no. 5, Oct. 2007.

[16] J. F. Liu, W. Tang, M. Wang, H. C. Zhang, H. F. Ma, X. Fu, and T. J. Cui, "A dual-mode UWB antenna for pattern diversity application," *IEEE Transactions on Antennas and Propagation*, vol. 68, no. 4, pp. 3219-3224, Apr. 2020.

[17] P. Liu, W. Jiang, S. Sun, Y. Xi, and S. Gong, "Broadband and low-profile penta-polarization reconfigurable metamaterial antenna," *IEEE Access*, vol. 8, pp. 21823-21831, 2020.

[18] G. Gao, R.-F. Zhang, W.-F. Geng, H.-J. Meng, and B. Hu, "Characteristic mode analysis of a non uniform metasurface antenna for wearable applications," *IEEE Antennas and Wireless Propagation Letters*, vol. 19, no. 8, pp. 1355-1359, Aug. 2020.

[19] A. Hiken, *Aerospace Engineering - 'The Evolution of the Composite Fuselage: A Manufacturing Perspective*, IntechOpen, Nov. 20, 2019.

J. Monica completed her B.E. degree in Electronics and Communication Engineering from Anna University in 2013 and M.E. degree in Communication Systems under Anna University in 2015. Currently pursuing her Ph.D. from Anna University, Chennai, India. Her research works is in the areas of Antennas and wireless propagations, Aircraft antennas, Microwave design and conformal antenna design. She has published papers in SCI indexed International journals and conferences.

P. Jothilakshmi completed her B.E. degree in Electronics and Communication Engineering from University of Madras, in 1996 and M.E. degree in Communication Systems from Madurai Kamaraj University, in 2000. She completed her Ph.D. degree from Anna University, Chennai, India. She is serving as a Teacher from 1996 onwards. She is currently serving as a Professor in ECE at Sri Venkateswara College of Engineering, Chennai, India. She is an active fellow in professional societies ISTE, IETE and IAENG. She lead several numbers of B.E. and M.E. and Ph.D. level project. She has published several SCI indexed; Scopus indexed International journal papers. She presented and published papers in International and National Conference. Her research area is Microwave antenna design and Wireless Communication.